EUROPEAN ORGANIZATION FOR NUCLEAR RESEARCH

CERN-EP/99-119
August 26, 1999

Study of Z Boson Pair Production in e^+e^- Collisions at LEP at $\sqrt{s} = 189$ GeV

The L3 Collaboration

Abstract

The pair production of Z bosons is studied using the data collected by the L3 detector at LEP in 1998 in e^+e^- collisions at a centre–of–mass energy of 189 GeV. All the visible final states are considered and the cross section of this process is measured to be $0.74^{+0.15}_{-0.14}\,(\text{stat.}) \pm 0.04\,(\text{syst.})$ pb. Final states containing b quarks are enhanced by a dedicated selection and their production cross section is found to be $0.18^{+0.09}_{-0.07}\,(\text{stat.}) \pm 0.02\,(\text{syst.})$ pb. Both results are in agreement with the Standard Model predictions. Limits on anomalous couplings between neutral gauge bosons are derived from these measurements.

Submitted to *Phys. Lett. B*

1 Introduction

Since 1997 LEP is running at centre–of–mass energies, $\sqrt{s}$, above the production threshold of Z boson pairs. This process is of particular interest as it constitutes an irreducible background for the search of the Standard Model Higgs boson and to several other processes predicted by theories beyond the Standard Model. In addition it allows the investigation of possible triple neutral gauge boson couplings, ZZZ and ZZγ [1], forbidden at tree level in the Standard Model.

The experimental investigation of ZZ production is made difficult by its rather low cross section, compared with competing processes that constitute large and sometimes irreducible backgrounds. The existence at threshold of this process was established at $\sqrt{s} = 183$ GeV [2]. In the following, the analysis of the data collected at 189 GeV is described. The measurement of the cross section is presented together with that of final states containing b quarks. Limits on anomalous couplings among neutral gauge bosons are derived.

2 Data and Monte Carlo Samples

The data were collected in 1998 by the L3 detector [3] at $\sqrt{\mathrm{s}} = 188.7$ GeV, and amount to an integrated luminosity of 176 pb^{-1}. This energy will be denoted as 189 GeV in the following.

The EXCALIBUR [4] Monte Carlo is used to generate events belonging to both the signal and the background neutral–current four–fermion processes. Background from fermion–pair production is described making use of PYTHIA 5.72 [5] ($\mathrm{e^+e^-} \rightarrow \mathrm{q\bar{q}}(\gamma)$), KORALZ 4.02 [6] ($\mathrm{e^+e^-} \rightarrow \mu^+\mu^-(\gamma)$ and $\mathrm{e^+e^-} \rightarrow \tau^+\tau^-(\gamma)$) and BHWIDE [7] ($\mathrm{e^+e^-} \rightarrow \mathrm{e^+e^-}(\gamma)$). Background from charged–current four–fermion processes is generated with EXCALIBUR for $\mathrm{e}\nu_\mathrm{e}\mathrm{q\bar{q}}'$ and $\ell^+\nu_\ell\ell^-\bar{\nu}_\ell$ with $\ell = \mathrm{e}, \mu, \tau$ and KORALW 1.21 [8] for WW production. Contributions from multiperipheral processes are modelled by PHOJET 1.05c [9] ($\mathrm{e^+e^-} \rightarrow \mathrm{e^+e^-q\bar{q}}$) and DIAG36 [10] ($\mathrm{e^+e^-} \rightarrow \mathrm{e^+e^-}\ell^+\ell^-$).

The L3 detector response is simulated using the GEANT 3.15 program [11], which takes into account the effects of energy loss, multiple scattering and showering in the detector. Time dependent detector inefficiencies, as measured in the data taking period, are reproduced in these simulations.

The definition of the Z pair signal is unchanged with respect to the generator level phase–space cuts of the 183 GeV analysis [2]. Those requirements are summarised as follows: the invariant mass of both the generated fermion pairs must be between 70 GeV and 105 GeV. This criterion has to be satisfied by at least one of the two possible pairings of four same flavour fermions. In the case in which fermion pairs can originate from a charged–current process ($\mathrm{u\bar{u}d\bar{d}}$, $\mathrm{c\bar{c}s\bar{s}}$ and $\nu_\ell\bar{\nu}_\ell\ell^+\ell^-$, with $\ell = \mathrm{e}, \mu, \tau$) the masses of the fermion pairs which could come from W decays are required to be either below 75 GeV or above 85 GeV. Events with electrons in the final state are rejected if $|\cos\theta_\mathrm{e}| > 0.95$, where θ_e is the electron polar angle.

The expected cross sections for the different final states are computed with EXCALIBUR. A total cross section of 0.662 pb is expected. In this calculation $\alpha_s = 0.119$ [12] is included for the QCD vertex corrections. The cross section for states with at least one b–quark pair amounts to 0.178 pb.

3 Event Selection

All the visible final states of the Z pair decay are investigated, with criteria similar to those used at 183 GeV [2]. All selections are based on the identification of two fermion pairs each with a mass close to the Z boson mass. The selections are modified to take into account the different background composition at the higher $\sqrt{s}$ and the changed signal topology due to the larger boost of the Z bosons. This boost leads to acollinear and acoplanar fermion pairs.

3.1 $\mathrm{q\bar{q}}\ell^+\ell^-$ Channel

A dedicated selection is performed for each of the final states $\mathrm{q\bar{q}e^+e^-}$, $\mathrm{q\bar{q}}\mu^+\mu^-$ and $\mathrm{q\bar{q}}\tau^+\tau^-$ after the application of a common preselection. This requires at least five charged tracks, 15 calorimetric clusters and a visible energy of more than $0.4\sqrt{s}$ together with two same flavour identified leptons.

Electrons are identified from energy depositions in the electromagnetic calorimeter whose shower shape is compatible with those initiated by an electron or a photon. At least one electron should have a matched track. Muons are reconstructed from tracks in the muon spectrometer pointing to the interaction vertex. Energy depositions in the calorimeters consistent with a minimum ionising particle (MIP) which have an associated track are also accepted as second muon candidates. For the $\mathrm{q\bar{q}}\tau^+\tau^-$ channel both a particle–based and a jet–based selection are performed. In the first, tau leptons are identified via their decay into isolated electrons or muons, or as an isolated low–multiplicity jet with one or three tracks and unit charge. In the jet–based selection, the event is forced into four–jets using the DURHAM [13] algorithm. Two of the jets must each have less than four tracks. These jets are considered as tau candidates, but at least one of them must coincide with a tau candidate defined in the particle–based selection.

In the electron and the muon channels both the lepton and the jet pair must have an opening angle of at least 120°, tightened to 130° for the taus. The invariant mass of the jet–jet and the lepton–lepton system after performing a kinematic fit, which imposes energy and momentum conservation, must be within 70 GeV and 120 GeV. The events are then subject to the DURHAM algorithm requiring $\ln\mathrm{Y}_{34}$ to be greater than -6.0 for the electron and tau channels and -6.5 for the muon one. Y_{34} is the jet resolution parameter for which the event is changed from a four–jet to a three–jet topology. Furthermore, the visible energy in the electron channel must be at least $0.8\sqrt{s}$ and between $0.6\sqrt{s}$ and $0.9\sqrt{s}$ for the jet–based tau selection.

Additional requirements are applied in the tau selection to reduce the radiative $\mathrm{q\bar{q}}(\gamma)$ background rejecting events containing a photon of energy larger than 30 GeV. Semileptonic WW events are rejected by requiring the transverse missing momentum to be lower than 40 GeV in events with no identified electron or muon with energy larger than 40 GeV.

The kinematic fit is repeated on events that pass at least one of the four selections described above with the extra constraint of equal invariant masses for the jet–jet and lepton–lepton systems. The distribution of the invariant mass arising from the fit, M_{5C}, is shown in Figure 1. Table 1 summarises the yield of this selection.

3.2 $\mathrm{q\bar{q}}\nu\bar{\nu}$ Channel

High multiplicity hadronic events with more than three charged tracks and at least 15 calorimetric energy clusters are selected. The event invariant mass must exceed 50 GeV. These cuts reduce contributions from purely leptonic two–fermion final states, as well as two–photon interactions, while keeping a significant fraction of hadronic events from $\mathrm{q\bar{q}}(\gamma)$ and W–pair

Selection	Data	Signal MC	Background MC	Efficiency
$\mathrm{q\bar{q}}\ell^+\ell^-$	15	10.9 ± 0.2	5.4 ± 0.2	61%
$\mathrm{q\bar{q}}\nu\bar{\nu}$	40	15.7 ± 0.5	18.9 ± 0.8	49%
$\ell^+\ell^-\nu\bar{\nu}$	3	0.7 ± 0.1	1.2 ± 0.1	22%
$\ell^+\ell^-\ell'^+\ell'^-$	2	0.7 ± 0.0	0.6 ± 0.1	37%
$\mathrm{q\bar{q}q'\bar{q}'}$	163	24.2 ± 0.4	153.0 ± 1.2	43%

Table 1: Data, signal and background Monte Carlo events selected by each analysis and their efficiency. The $\mathrm{q\bar{q}}\nu\bar{\nu}$ entries are reported for a selection requirement of 0.5 on the neural network output. The $\ell^+\ell^-\nu\bar{\nu}$ figures refer only to electrons and muons. The Monte Carlo statistical uncertainties are given on signal and background expectations.

production. These latter contributions are further reduced by requiring the visible mass to be less than 130 GeV and the mass recoiling against the hadronic system to exceed 50 GeV.

In addition, the transverse momentum is required to be greater than 5 GeV and the longitudinal momentum to be smaller than 40% of the visible energy. The energy deposition in the forward calorimeters must not exceed 10 GeV and the missing momentum vector must be at least 16° away from the beam axis. No electrons, muons or photons with energies above 20 GeV are allowed in the event and the energy in a 25° azimuthal sector around the missing energy direction, E_{25}, is required to be smaller than 30 GeV.

A total of 299 events satisfy the selection criteria with 23 and 266 events expected from the signal and background Monte Carlo simulations respectively. The dominating background is due to charged–current four–fermion processes. To differentiate further the ZZ signal from the remaining background a neural network is constructed. The inputs to the neural network include event shape variables which help to distinguish two–jet from three–jet topologies, the sum of invariant and missing masses, the masses of the two jets, the total missing momentum and E_{25}. The use of the neural network increases the signal fraction in the selected sample to approximately 60% for large neural network output values, as demonstrated in Figure 2a. The efficiency and the yield of this selection are reported in Table 1 for a cut at 0.5, while the full spectrum is used for the cross section determination.

3.3 $\ell^+\ell^-\nu\bar{\nu}$ Channel

The selection for $\ell^+\ell^-\nu\bar{\nu}$ is optimised for electron and muon pairs identified as in Section 3.1 and characterised by an invariant mass, $M_{\ell\ell}$, between 85 GeV and 95 GeV. The requirement on the associated track for electrons is dropped and MIPs are not considered.

In the electron channel only events with a visible energy between 75 GeV and 98 GeV are selected; this requirement is loosened to the range 65 GeV − 140 GeV for muons. The opening angle of the two electrons must be below 166° and from 143° to 172° for the two muons. In order to reduce the background from radiative Bhabha scattering and purely leptonic decays of W pairs, the recoil mass to the electron pair is required to be less than 95 GeV. The background from other resonant and non–resonant four–fermion processes is reduced by performing a kinematic fit imposing the Z mass to the visible pair of leptons and recalculating their four–momenta. The recoil mass, M_{rec}, after the fit is required to be less than 98 GeV for electrons and in excess of 84 GeV but not larger than 98 GeV for muons. The transverse momentum has to lie in the range from 4 GeV to 29 GeV.

The spectrum of the sum of $M_{\ell\ell}$ and M_{rec}, without applying the kinematic fit, peaked around twice the Z mass is presented in Figure 2b. Table 1 lists the efficiencies and the yield of the selection. No contribution in the $\tau^+\tau^-\nu_\tau\bar{\nu}_\tau$ signal channel is expected.

3.4 $\ell^+\ell^-\ell'^+\ell'^-$ Channel

This selection is based on events with at least four loosely identified leptons of a minimum energy of 3 GeV and the subsequent study of just one pair of them.

First a low multiplicity event preselection is applied, requiring at least two tracks but less than 15 calorimetric clusters, with a total visible energy between $0.2\sqrt{s}$ and $1.3\sqrt{s}$. Electrons and muons are identified as described in Section 3.1. Low angle electromagnetic showers ($|\cos\theta| > 0.95$) without a matching track are also accepted as electrons. Tau candidates are identified as low multiplicity hadronic jets with either one or three tracks in a cone of $10°$ half opening angle. To reject hadronic jets, the energy between $10°$ and $30°$ around the tau direction must not exceed half of the energy in a cone of $10°$ half opening angle. To increase the selection efficiency, MIPs are also accepted.

If there are more than four lepton candidates, the four most consistent with energy and momentum conservation are chosen. Events are then required to have at least one electron, muon, tau or muon–MIP pair. Low angle electrons are not considered in this procedure. If more than one such pair is possible, the one with the invariant mass, $M_{\ell\ell}$, closest to the Z mass is chosen.

Both $M_{\ell\ell}$ and the recoil mass, M_{rec}, to this selected lepton pair are required to lie between 70 GeV and 105 GeV. The data and Monte Carlo distributions for $M_{\ell\ell} + M_{rec}$ are shown in Figure 2c. Table 1 summarises the total yield of the selection.

3.5 $\mathrm{q\bar{q}q'\bar{q}'}$ Channel

The four–jet selection has to cope with the large QCD and W pair production backgrounds. High multiplicity hadronic events are selected by requiring a visible energy between $0.6\sqrt{s}$ and $1.4\sqrt{s}$ together with parallel and perpendicular imbalances below $0.3\sqrt{s}$. Events with an identified electron, muon or photon with energy in excess of 65 GeV are discarded.

The events forced to four jets with the DURHAM algorithm are subjected to a constrained fit which rescales the jets to balance momentum while imposing energy conservation. This fit reduces greatly the dependence on the calorimeter energy scale. A first neural network [14] is then applied to distinguish events with four genuine quark jets from those with two quark jets and two jets from gluon radiation. A cut on the output of this neural network rejects QCD background selecting a hadronic sample enhanced in W and Z pairs.

A second network uses five variables to distinguish Z pairs from W pairs by means of their mass difference after the dijet pairings are chosen to minimise the dijet mass difference. The variables are the reconstructed dijet mass, the maximum and minimum energy in any jet, the average number of charged tracks per jet and the dijet mass difference. A large portion of four–jet ZZ decays contains at least one b quark pair, which provides significant distinguishing power from W pair decays. A sixth variable, a b–tag discriminant [15], is added to the network. The output of this network is shown in Figure 2d. A cut on the background enhanced region below 0.2 is applied and the rise above 0.8 is due to the b–tagged events. The performances of the analysis are summarised in Table 1.

A simpler sequential analysis is also performed for this channel, taking advantage of the different boost of Z and W pairs and hence investigating just the two dijet opening angles, the dijet mass difference and the dijet mean mass. Results compatible with the previous approach are obtained limited by a lower purity due to the absence of b–tagging.

4 Measurement of the ZZ Cross Section

A binned maximum likelihood fit to each of the variables displayed in Figures 1 and 2 allows the determination of the ZZ cross section in the individual final states, as listed in Table 2. These are in agreement with the Standard Model values reported in the same table. Assuming these predictions as the relative weights of different channels, the ZZ cross section, σ_{ZZ}, is found to be:

$$\sigma_{\mathrm{ZZ}} = 0.74^{+0.15}_{-0.14}\,\mathrm{pb},$$

in good agreement with the expected cross section within the signal definition cuts of 0.662 pb. The uncertainties are only statistical.

In the calculation of the cross section the effect of the cross talk between the separate channels is found to be negligible.

	$\mathrm{q\bar{q}}\ell^+\ell^-$	$\mathrm{q\bar{q}}\nu\bar{\nu}$	$\ell^+\ell^-\nu\bar{\nu}$	$\ell^+\ell^-\ell'^+\ell'^-$	$\mathrm{q\bar{q}q'\bar{q}'}$
Measured cross section (pb)	$0.096^{+0.039}_{-0.033}$	$0.23^{+0.07}_{-0.06}$	$0.054^{+0.059}_{-0.040}$	$0.017^{+0.025}_{-0.015}$	$0.32^{+0.14}_{-0.13}$
Expected cross section (pb)	0.102	0.179	0.027	0.011	0.316

Table 2: Result of the individual cross section fits.

5 Study of Systematic Errors

The systematic uncertainties are grouped in correlated and uncorrelated sources among the channels. The correlated sources of systematic errors are the background cross sections, the LEP energy and the energy scale of the detector. As they modify the shapes of the investigated distributions, their effect is evaluated performing a new fit to calculate σ_{ZZ} once their values are scaled to the extremes listed in Table 3. An uncertainty of 2% is attributed to the measured cross section to take into account the difference of the assumed relative weights of the different channels with respect to those obtained with the GRC4F [16] Monte Carlo generator and to parametrise the other uncertainties related to their calculation.

Four sources of systematic uncertainty are uncorrelated among the channels and modify the shapes of some of the discriminating distributions. The jet resolution and the charged track multiplicity for the $\mathrm{q\bar{q}q'\bar{q}'}$ selection are scaled as in Table 3. The b–tag procedure and the Monte Carlo description of b–hadron jets are taken into account by reweighting the value of the b–tag discriminant. Finally the Bhabha Monte Carlo is not sufficient to estimate the background to the $\ell^+\ell^-\nu\bar{\nu}$ channel. This estimate is obtained from a fit to the shapes of some selection variables whose uncertainty contributes to the total systematic uncertainty. Two additional sources of systematic uncertainty are propagated to the total cross section: the Monte Carlo statistics and lepton identification. Their uncertainties listed in Table 4 do not affect the shape of the discriminating distributions.

The individual and combined systematic errors are listed in Table 3.

The measured cross section is then:

$$\sigma_{\mathrm{ZZ}} = 0.74^{+0.15}_{-0.14}\,(\mathrm{stat.})\pm 0.04\,(\mathrm{syst.})\,\mathrm{pb}.$$

Systematic Source	Variation	$\delta\sigma_{\mathrm{ZZ}}$ (pb)	$\delta\sigma_{\mathrm{ZZ}\to\mathrm{b\bar{b}X}}$ (pb)
Correlated sources			
Lep energy	40 MeV	< 0.01	< 0.01
WW cross section	2%	0.01	< 0.01
Four–jet rate	5%	0.01	0.01
Weν cross section	10%	0.01	< 0.01
Four–fermion cross section	5%	< 0.01	0.01
Energy scale	2%	0.01	0.01
Theory predictions	2%	0.01	< 0.01
Uncorrelated sources			
Jet resolution ($\mathrm{q\bar{q}q'\bar{q}'}$)	2%	0.01	< 0.01
Charge multiplicity ($\mathrm{q\bar{q}q'\bar{q}'}$)	1%	< 0.01	< 0.01
B–tag ($\mathrm{q\bar{q}q'\bar{q}'}$)	see text	0.01	0.01
Bhabha background ($\ell^+\ell^-\nu\bar{\nu}$)	see text	0.01	–
Monte Carlo statistics	see text	0.02	0.01
Lepton identification	see text	0.01	0.01
Total		0.04	0.02

Table 3: Systematic uncertainties on σ_{ZZ} and $\sigma_{\mathrm{ZZ}\to\mathrm{b\bar{b}X}}$.

Channel	Systematic Source	Background uncertainty	Signal uncertainty
$\mathrm{q\bar{q}}\ell^+\ell^-$	Monte Carlo statistics	4.7%	1.7%
	Lepton identification	2.7%	4.1%
$\mathrm{q\bar{q}}\nu\bar{\nu}$	Monte Carlo statistics	4.0%	3.0%
$\ell^+\ell^-\nu\bar{\nu}$	Monte Carlo statistics	8.0%	8.0%
	Lepton identification	5.0%	4.0%
$\ell^+\ell^-\ell'^+\ell'^-$	Monte Carlo statistics	21.4%	2.1%
	Lepton identification	10.1%	4.3%
$\mathrm{q\bar{q}q'\bar{q}'}$	Monte Carlo statistics	0.8%	1.7%

Table 4: Sources of uncorrelated systematic uncertainties.

In terms of the NC02 cross section in which only the two conversion diagrams are considered for the double–resonant Z pair production, the cross section reads

$$\sigma^{\mathrm{NC02}}_{\mathrm{ZZ}} = 0.73^{+0.15}_{-0.14}\,(\mathrm{stat.})\pm 0.04\,(\mathrm{syst.})\,\mathrm{pb},$$

to be compared with a Standard Model expectation of 0.65 pb calculated with the YFSZZ [17] package.

6 b Quark Content in ZZ Events

It is of particular interest to investigate the rate of ZZ events with b quark content. The production of the minimal or a supersymmetric Higgs boson would manifest via an enhancement of these events and their study complements the dedicated search for such processes [15]. The expected Standard Model cross section for $\mathrm{ZZ}\rightarrow \mathrm{b\bar{b}X}$ final states is 0.178 pb.

The investigation of the $\mathrm{ZZ}\rightarrow \mathrm{b\bar{b}X}$ events proceeds by complementing the analyses of the $\mathrm{q\bar{q}}\nu\bar{\nu}$ and $\mathrm{q\bar{q}}\ell^+\ell^-$ final states described above with a further variable describing the b quark content in the event [15]. Three variables are then considered for each final state: M_{5C} for the $\mathrm{q\bar{q}}\ell^+\ell^-$ and the neural network output for the $\mathrm{q\bar{q}}\nu\bar{\nu}$ analysis together with the b–tag evaluated for each of the two hadronic jets. The combination of each of the sets of these three variables into a single discriminant proceeds as follows. First the variables are mapped to achieve uniform distributions for the background. Then the product of their observed values is calculated event by event. Finally the confidence level is calculated for the product of three uniformly distributed quantities to be less than the observed product. This confidence level is expected to be low for signal and flat for background. The final discriminant is the negative logarithm of this confidence level and is shown in Figure 3. Figure 2d shows the $\mathrm{b\bar{b}q\bar{q}}$ response from the neural network used to select the $\mathrm{q\bar{q}q'\bar{q}'}$ final states.

The cross section calculation is performed as above. Results for the individual channels are listed in Table 5. The combined result for $\sigma_{\mathrm{ZZ}\rightarrow\mathrm{b\bar{b}X}}$ is:

$$\sigma_{\mathrm{ZZ}\rightarrow\mathrm{b\bar{b}X}} = 0.18^{+0.09}_{-0.07}\,(\mathrm{stat.})\ \pm 0.02\,(\mathrm{syst.})\,\mathrm{pb}.$$

This result agrees with the Standard Model expectation and differs from zero at 99.9% confidence level. In the fit the other ZZ final states are fixed to their Standard Model expectations. The systematic uncertainties are evaluated in the same way as for the total cross section and are presented in Table 3. Figure 4 displays the measured total and $\mathrm{b\bar{b}X}$ cross sections and their expected evolution with $\sqrt{s}$.

	$\mathrm{b\bar{b}}\ell^+\ell^-$	$\mathrm{b\bar{b}}\nu\bar{\nu}$	$\mathrm{q\bar{q}b\bar{b}}$
Measured cross section (pb)	$0.020^{+0.022}_{-0.014}$	$0.044^{+0.046}_{-0.036}$	$0.111^{+0.076}_{-0.062}$
Expected cross section (pb)	0.021	0.039	0.118

Table 5: Result of the individual $\mathrm{ZZ}\rightarrow \mathrm{b\bar{b}X}$ cross section fits.

7 Anomalous Couplings

A parametrisation of the ZZZ and ZZγ anomalous couplings is given in Reference [1]. Assuming on-shell production of a pair of Z bosons, only four couplings f_i^{V} ($i = 4,5; \mathrm{V} = \gamma, \mathrm{Z}$), where the V superscript corresponds to an anomalous coupling ZZV, may be different from zero. At tree level these couplings are zero in the Standard Model. They are independent from the h_i^{Z} couplings that parametrise the possible anomalous ZZγ vertex [1], probed by the $\mathrm{e^+e^-} \rightarrow \mathrm{Z}\gamma$ process [18].

In order to calculate the impact of anomalous couplings on the measured distributions in the process $\mathrm{e^+e^-} \rightarrow \mathrm{f\bar{f}f'\bar{f}'}$, the EXCALIBUR generator is extended [19]. The matrix elements of the Standard Model are supplemented by an additional term containing anomalous couplings,

$\mathcal{M}_{\rm AC}(\{p^\nu\},\lambda,f_i^{\rm V})$ [1], where $\{p^\nu\}$ represents the phase space variables and λ the helicities of initial and final state fermions. Four–fermion Monte Carlo distributions for non–zero anomalous couplings are then obtained by reweighting each event with the factor

$$W(\{p^\nu\},f_i^{\rm V}) \equiv \frac{\frac{1}{4}\sum\limits_{\lambda}\Big|(\mathcal{M}_{\rm 4f}(\{p^\nu\},\lambda)+\mathcal{M}_{\rm AC}(\{p^\nu\},\lambda,f_i^{\rm V}))\ \Big|^2}{\frac{1}{4}\sum\limits_{\lambda}|\mathcal{M}_{\rm 4f}(\{p^\nu\},\lambda)\ |^2},$$

where $\mathcal{M}_{\rm 4f}(\{p^\nu\},\lambda)$ is the Standard Model amplitude for the four–fermion final states. An average over initial state and a sum over final state helicities are carried out. Initial state radiation is taken into account by evaluating the event weight at the centre–of–mass of the four–fermion system. Figure 1 displays the effects of an anomalous value of f_4^γ obtained by reweighting with this technique the four–fermion Monte Carlo events selected by the $\rm q\bar{q}\ell^+\ell^-$ analysis.

The effects of anomalous couplings not only change the ZZ cross section but also the shape of the distributions. Using the distributions given in Figures 1 and 2, a binned maximum likelihood fit is therefore performed for each of the anomalous couplings $f_i^{\rm V}$, fixing the others to zero.

The results of all these fits are compatible with the Standard Model and 95% confidence level limits on the couplings are set as follows:

$$-1.9 \leq f_4^{\rm Z} \leq 1.9;\quad -5.0 \leq f_5^{\rm Z} \leq 4.5;\quad -1.1 \leq f_4^\gamma \leq 1.2;\quad -3.0 \leq f_5^\gamma \leq 2.9.$$

These limits are still valid for off–shell ZZ production where additional couplings are possible. The small asymmetries in these limits are due to the interference term between the anomalous coupling diagram and the Standard Model diagrams. Systematic uncertainties on signal and background cross sections are taken into account in the derivation of the limits.

These limits improve by nearly a factor two previously published results at $\sqrt{s}=183$ GeV [2], which are included in the present analysis.

Acknowledgements

We thank the CERN accelerator divisions for the excellent performance and the continuous and successful upgrade of the LEP machine. We acknowledge the contributions of the engineers and technicians who have participated in the construction and maintenance of this experiment.

References

[1] K. Hagiwara *et al.*, Nucl. Phys. **B 282** (1987) 253.

[2] L3 Collab., M. Acciarri *et al.*, Phys. Lett. **B 450** (1999) 281.

[3] L3 Collab., B. Adeva *et al.*, Nucl. Inst. Meth. **A 289** (1990) 35; L3 Collab., O. Adriani *et al.*, Physics Reports **236** (1993) 1; I. C. Brock *et al.*, Nucl. Instr. and Meth. **A 381** (1996) 236; M. Chemarin *et al.*, Nucl. Inst. Meth. **A 349** (1994) 345; M. Acciarri *et al.*, Nucl. Inst. Meth. **A 351** (1994) 300; A. Adam *et al.*, Nucl. Inst. Meth. **A 383** (1996) 342; G. Basti *et al.*, Nucl. Inst. Meth. **A 374** (1996) 293.

[4] F.A. Berends, R. Kleiss and R. Pittau, Nucl. Phys. **B 424** (1994) 308; Nucl. Phys. **B 426** (1994) 344; Nucl. Phys. (Proc. Suppl.) **B 37** (1994) 163; R. Kleiss and R. Pittau, Comp. Phys. Comm. **85** (1995) 447; R. Pittau, Phys. Lett. **B 335** (1994) 490.

[5] T. Sjöstrand, CERN–TH/7112/93 (1993), revised August 1995; T. Sjöstrand, Comp. Phys. Comm. **82** (1994) 74.

[6] S. Jadach, B.F.L. Ward and Z. Wąs, Comp. Phys. Comm **79** (1994) 503.

[7] S. Jadach *et al.*, Phys. Lett. **B 390** (1997) 298.

[8] M. Skrzypek *et al.*, Comp. Phys. Comm. **94** (1996) 216; M. Skrzypek *et al.*, Phys. Lett. **B 372** (1996) 289.

[9] R. Engel, Z Phys. **C 66** (1995) 203; R. Engel and J. Ranft, Phys. Rep. **D 54** (1996) 4244.

[10] F.A. Berends, P.H. Daverfelt and R. Kleiss, Nucl. Phys. **B 253** (1985) 441; Comp. Phys. Comm. **40** (1986) 285.

[11] The L3 detector simulation is based on GEANT Version 3.15. R. Brun *et al.*, "GEANT 3", CERN–DD/EE/84–1 (Revised), 1987. The GHEISHA program (H. Fesefeldt, RWTH Aachen Report PITHA 85/02 (1985)) is used to simulate hadronic interactions.

[12] Particle Data Group, C. Caso *et al.*, Eur. Phys. J. **C 3** (1998) 1.

[13] S. Bethke *et al.*, Nucl. Phys. **B 370** (1992) 310.

[14] L3 Collab., M. Acciarri *et al.*, Phys. Lett. **B 436** (1999) 437.

[15] L3 Collab., M. Acciarri *et al.*, Phys. Lett. **B 431** (1998) 437; L3 Collab., M. Acciarri *et al.*, Phys. Lett. **B 436** (1998) 403; L3 Collab., M. Acciarri *et al.*, CERN-EP/99-80, Submitted to Phys. Lett. B.

[16] J. Fujimoto *et al.*, Comp. Phys. Comm. **100** (1997) 128.

[17] S. Jadach, B.F.L. Ward and Z. Wąs, Phys. Rev. **D56** (1997) 6939.

[18] L3 Collab., M. Acciarri *et al.*, Phys. Lett. **B 436** (1998) 187.

[19] J. Alcaraz *et al.*, preprint hep-ph/9812435.

The L3 Collaboration:

M.Acciarri,[26] P.Achard,[19] O.Adriani,[16] M.Aguilar-Benitez,[25] J.Alcaraz,[25] G.Alemanni,[22] J.Allaby,[17] A.Aloisio,[28] M.G.Alviggi,[28] G.Ambrosi,[19] H.Anderhub,[47] V.P.Andreev,[6,36] T.Angelescu,[12] F.Anselmo,[9] A.Arefiev,[27] T.Azemoon,[3] T.Aziz,[10] P.Bagnaia,[35] L.Baksay,[42] A.Balandras,[4] R.C.Ball,[3] S.Banerjee,[10] Sw.Banerjee,[10] A.Barczyk,[47,45] R.Barillère,[17] L.Barone,[35] P.Bartalini,[22] M.Basile,[9] R.Battiston,[32] A.Bay,[22] F.Becattini,[16] U.Becker,[14] F.Behner,[47] L.Bellucci,[16] J.Berdugo,[25] P.Berges,[14] B.Bertucci,[32] B.L.Betev,[47] S.Bhattacharya,[10] M.Biasini,[32] A.Biland,[47] J.J.Blaising,[4] S.C.Blyth,[33] G.J.Bobbink,[2] A.Böhm,[1] L.Boldizsar,[13] B.Borgia,[35] D.Bourilkov,[47] M.Bourquin,[19] S.Braccini,[19] J.G.Branson,[38] V.Brigljevic,[47] F.Brochu,[4] A.Buffini,[16] A.Buijs,[43] J.D.Burger,[14] W.J.Burger,[32] J.Busenitz,[42] A.Button,[3] X.D.Cai,[14] M.Campanelli,[47] M.Capell,[14] G.Cara Romeo,[9] G.Carlino,[28] A.M.Cartacci,[16] J.Casaus,[25] G.Castellini,[16] F.Cavallari,[35] N.Cavallo,[28] C.Cecchi,[19] M.Cerrada,[25] F.Cesaroni,[23] M.Chamizo,[19] Y.H.Chang,[49] U.K.Chaturvedi,[18] M.Chemarin,[24] A.Chen,[49] G.Chen,[7] G.M.Chen,[7] H.F.Chen,[20] H.S.Chen,[7] X.Chereau,[4] G.Chiefari,[28] L.Cifarelli,[37] F.Cindolo,[9] C.Civinini,[16] I.Clare,[14] R.Clare,[14] G.Coignet,[4] A.P.Colijn,[2] N.Colino,[25] F.Conventi,[28] S.Costantini,[8] F.Cotorobai,[12] B.Cozzoni,[9] B.de la Cruz,[25] A.Csilling,[13] S.Cucciarelli,[32] T.S.Dai,[14] J.A.van Dalen,[30] R.D'Alessandro,[16] R.de Asmundis,[28] P.Déglon,[19] A.Degré,[4] K.Deiters,[45] M.Della Pietra,[28] D.della Volpe,[28] P.Denes,[34] F.DeNotaristefani,[35] A.De Salvo,[47] M.Diemoz,[35] D.van Dierendonck,[2] F.Di Lodovico,[47] C.Dionisi,[35] M.Dittmar,[47] A.Dominguez,[38] A.Doria,[28] M.T.Dova,[18,♯] D.Duchesneau,[4] D.Dufournaud,[4] P.Duinker,[2] I.Duran,[39] H.El Mamouni,[24] A.Engler,[33] F.J.Eppling,[14] F.C.Erné,[2] P.Extermann,[19] M.Fabre,[45] R.Faccini,[35] M.A.Falagan,[25] S.Falciano,[35,17] A.Favara,[17] J.Fay,[24] O.Fedin,[36] M.Felcini,[47] T.Ferguson,[33] F.Ferroni,[35] H.Fesefeldt,[1] E.Fiandrini,[32] J.H.Field,[19] F.Filthaut,[17] P.H.Fisher,[14] I.Fisk,[38] G.Forconi,[14] L.Fredj,[19] K.Freudenreich,[47] C.Furetta,[26] Yu.Galaktionov,[27,14] S.N.Ganguli,[10] P.Garcia-Abia,[5] M.Gataullin,[31] S.S.Gau,[11] S.Gentile,[35,17] N.Gheordanescu,[12] S.Giagu,[35] Z.F.Gong,[20] G.Grenier,[24] O.Grimm,[47] M.W.Gruenewald,[8] M.Guida,[37] R.van Gulik,[2] V.K.Gupta,[34] A.Gurtu,[10] L.J.Gutay,[44] D.Haas,[5] A.Hasan,[29] D.Hatzifotiadou,[9] T.Hebbeker,[8] A.Hervé,[17] P.Hidas,[13] J.Hirschfelder,[33] H.Hofer,[47] G. Holzner,[47] H.Hoorani,[33] S.R.Hou,[49] I.Iashvili,[46] B.N.Jin,[7] L.W.Jones,[3] P.de Jong,[2] I.Josa-Mutuberría,[25] R.A.Khan,[18] D.Kamrad,[46] M.Kaur,[18,◇] M.N.Kienzle-Focacci,[19] D.Kim,[35] D.H.Kim,[41] J.K.Kim,[41] S.C.Kim,[41] J.Kirkby,[17] D.Kiss,[13] W.Kittel,[30] A.Klimentov,[14,27] A.C.König,[30] A.Kopp,[46] I.Korolko,[27] V.Koutsenko,[14,27] M.Kräber,[47] R.W.Kraemer,[33] W.Krenz,[1] A.Kunin,[14,27] P.Ladron de Guevara,[25] I.Laktineh,[24] G.Landi,[16] K.Lassila-Perini,[47] P.Laurikainen,[21] A.Lavorato,[37] M.Lebeau,[17] A.Lebedev,[14] P.Lebrun,[24] P.Lecomte,[47] P.Lecoq,[17] P.Le Coultre,[47] H.J.Lee,[8] J.M.Le Goff,[17] R.Leiste,[46] E.Leonardi,[35] P.Levtchenko,[36] C.Li,[20] C.H.Lin,[49] W.T.Lin,[49] F.L.Linde,[2] L.Lista,[28] Z.A.Liu,[7] W.Lohmann,[46] E.Longo,[35] Y.S.Lu,[7] K.Lübelsmeyer,[1] C.Luci,[17,35] D.Luckey,[14] L.Lugnier,[24] L.Luminari,[35] W.Lustermann,[47] W.G.Ma,[20] M.Maity,[10] L.Malgeri,[17] A.Malinin,[27,17] C.Maña,[25] D.Mangeol,[30] J.Mans,[34] P.Marchesini,[47] G.Marian,[15] J.P.Martin,[24] F.Marzano,[35] G.G.G.Massaro,[2] K.Mazumdar,[10] R.R.McNeil,[6] S.Mele,[17] L.Merola,[28] M.Meschini,[16] W.J.Metzger,[30] M.von der Mey,[1] A.Mihul,[12] H.Milcent,[17] G.Mirabelli,[35] J.Mnich,[17] G.B.Mohanty,[10] P.Molnar,[8] B.Monteleoni,[16,†] T.Moulik,[10] G.S.Muanza,[24] F.Muheim,[19] A.J.M.Muijs,[2] M.Musy,[35] M.Napolitano,[28] F.Nessi-Tedaldi,[47] H.Newman,[31] T.Niessen,[1] A.Nisati,[35] H.Nowak,[46] Y.D.Oh,[41] G.Organtini,[35] R.Ostonen,[21] C.Palomares,[25] D.Pandoulas,[1] S.Paoletti,[35,17] P.Paolucci,[28] R.Paramatti,[35] H.K.Park,[33] I.H.Park,[41] G.Pascale,[35] G.Passaleva,[17] S.Patricelli,[28] T.Paul,[11] M.Pauluzzi,[32] C.Paus,[17] F.Pauss,[47] D.Peach,[17] M.Pedace,[35] S.Pensotti,[26] D.Perret-Gallix,[4] B.Petersen,[30] D.Piccolo,[28] F.Pierella,[9] M.Pieri,[16] P.A.Piroué,[34] E.Pistolesi,[26] V.Plyaskin,[27] M.Pohl,[47] V.Pojidaev,[27,16] H.Postema,[14] J.Pothier,[17] N.Produit,[19] D.O.Prokofiev,[44] D.Prokofiev,[36] J.Quartieri,[37] G.Rahal-Callot,[47,17] M.A.Rahaman,[10] P.Raics,[15] N.Raja,[10] R.Ramelli,[47] P.G.Rancoita,[26] G.Raven,[38] P.Razis,[29] D.Ren,[47] M.Rescigno,[35] S.Reucroft,[11] T.van Rhee,[43] S.Riemann,[46] K.Riles,[3] A.Robohm,[47] J.Rodin,[42] B.P.Roe,[3] L.Romero,[25] A.Rosca,[8] S.Rosier-Lees,[4] J.A.Rubio,[17] D.Ruschmeier,[8] H.Rykaczewski,[47] S.Sarkar,[35] J.Salicio,[17] E.Sanchez,[17] M.P.Sanders,[30] M.E.Sarakinos,[21] C.Schäfer,[1] V.Schegelsky,[36] S.Schmidt-Kaerst,[1] D.Schmitz,[1] H.Schopper,[48] D.J.Schotanus,[30] G.Schwering,[1] C.Sciacca,[28] D.Sciarrino,[19] A.Seganti,[9] L.Servoli,[32] S.Shevchenko,[31] N.Shivarov,[40] V.Shoutko,[27] E.Shumilov,[27] A.Shvorob,[31] T.Siedenburg,[1] D.Son,[41] B.Smith,[33] P.Spillantini,[16] M.Steuer,[14] D.P.Stickland,[34] A.Stone,[6] H.Stone,[34,†] B.Stoyanov,[40] A.Straessner,[1] K.Sudhakar,[10] G.Sultanov,[18] L.Z.Sun,[20] H.Suter,[47] J.D.Swain,[18] Z.Szillasi,[42,¶] T.Sztaricshai,[42,¶] X.W.Tang,[7] L.Tauscher,[5] L.Taylor,[11] C.Timmermans,[30] Samuel C.C.Ting,[14] S.M.Ting,[14] S.C.Tonwar,[10] J.Tóth,[13] C.Tully,[34] K.L.Tung,[7] Y.Uchida,[14] J.Ulbricht,[47] E.Valente,[35] G.Vesztergombi,[13] I.Vetlitsky,[27] D.Vicinanza,[37] G.Viertel,[47] S.Villa,[11] M.Vivargent,[4] S.Vlachos,[5] I.Vodopianov,[36] H.Vogel,[33] H.Vogt,[46] I.Vorobiev,[27] A.A.Vorobyov,[36] A.Vorvolakos,[29] M.Wadhwa,[5] W.Wallraff,[1] M.Wang,[14] X.L.Wang,[20] Z.M.Wang,[20] A.Weber,[1] M.Weber,[1] P.Wienemann,[1] H.Wilkens,[30] S.X.Wu,[14] S.Wynhoff,[1] L.Xia,[31] Z.Z.Xu,[20] B.Z.Yang,[20] C.G.Yang,[7] H.J.Yang,[7] M.Yang,[7] J.B.Ye,[20] S.C.Yeh,[50] An.Zalite,[36] Yu.Zalite,[36] Z.P.Zhang,[20] G.Y.Zhu,[7] R.Y.Zhu,[31] A.Zichichi,[9,17,18] F.Ziegler,[46] G.Zilizi,[42,¶] M.Zöller.[1]

1 I. Physikalisches Institut, RWTH, D-52056 Aachen, FRG§
III. Physikalisches Institut, RWTH, D-52056 Aachen, FRG§
2 National Institute for High Energy Physics, NIKHEF, and University of Amsterdam, NL-1009 DB Amsterdam, The Netherlands
3 University of Michigan, Ann Arbor, MI 48109, USA
4 Laboratoire d'Annecy-le-Vieux de Physique des Particules, LAPP,IN2P3-CNRS, BP 110, F-74941 Annecy-le-Vieux CEDEX, France
5 Institute of Physics, University of Basel, CH-4056 Basel, Switzerland
6 Louisiana State University, Baton Rouge, LA 70803, USA
7 Institute of High Energy Physics, IHEP, 100039 Beijing, China△
8 Humboldt University, D-10099 Berlin, FRG§
9 University of Bologna and INFN-Sezione di Bologna, I-40126 Bologna, Italy
10 Tata Institute of Fundamental Research, Bombay 400 005, India
11 Northeastern University, Boston, MA 02115, USA
12 Institute of Atomic Physics and University of Bucharest, R-76900 Bucharest, Romania
13 Central Research Institute for Physics of the Hungarian Academy of Sciences, H-1525 Budapest 114, Hungary‡
14 Massachusetts Institute of Technology, Cambridge, MA 02139, USA
15 Lajos Kossuth University-ATOMKI, H-4010 Debrecen, Hungary¶
16 INFN Sezione di Firenze and University of Florence, I-50125 Florence, Italy
17 European Laboratory for Particle Physics, CERN, CH-1211 Geneva 23, Switzerland
18 World Laboratory, FBLJA Project, CH-1211 Geneva 23, Switzerland
19 University of Geneva, CH-1211 Geneva 4, Switzerland
20 Chinese University of Science and Technology, USTC, Hefei, Anhui 230 029, China△
21 SEFT, Research Institute for High Energy Physics, P.O. Box 9, SF-00014 Helsinki, Finland
22 University of Lausanne, CH-1015 Lausanne, Switzerland
23 INFN-Sezione di Lecce and Universitá Degli Studi di Lecce, I-73100 Lecce, Italy
24 Institut de Physique Nucléaire de Lyon, IN2P3-CNRS,Université Claude Bernard, F-69622 Villeurbanne, France
25 Centro de Investigaciones Energéticas, Medioambientales y Tecnologícas, CIEMAT, E-28040 Madrid, Spain♭
26 INFN-Sezione di Milano, I-20133 Milan, Italy
27 Institute of Theoretical and Experimental Physics, ITEP, Moscow, Russia
28 INFN-Sezione di Napoli and University of Naples, I-80125 Naples, Italy
29 Department of Natural Sciences, University of Cyprus, Nicosia, Cyprus
30 University of Nijmegen and NIKHEF, NL-6525 ED Nijmegen, The Netherlands
31 California Institute of Technology, Pasadena, CA 91125, USA
32 INFN-Sezione di Perugia and Universitá Degli Studi di Perugia, I-06100 Perugia, Italy
33 Carnegie Mellon University, Pittsburgh, PA 15213, USA
34 Princeton University, Princeton, NJ 08544, USA
35 INFN-Sezione di Roma and University of Rome, "La Sapienza", I-00185 Rome, Italy
36 Nuclear Physics Institute, St. Petersburg, Russia
37 University and INFN, Salerno, I-84100 Salerno, Italy
38 University of California, San Diego, CA 92093, USA
39 Dept. de Fisica de Particulas Elementales, Univ. de Santiago, E-15706 Santiago de Compostela, Spain
40 Bulgarian Academy of Sciences, Central Lab. of Mechatronics and Instrumentation, BU-1113 Sofia, Bulgaria
41 Center for High Energy Physics, Adv. Inst. of Sciences and Technology, 305-701 Taejon, Republic of Korea
42 University of Alabama, Tuscaloosa, AL 35486, USA
43 Utrecht University and NIKHEF, NL-3584 CB Utrecht, The Netherlands
44 Purdue University, West Lafayette, IN 47907, USA
45 Paul Scherrer Institut, PSI, CH-5232 Villigen, Switzerland
46 DESY, D-15738 Zeuthen, FRG
47 Eidgenössische Technische Hochschule, ETH Zürich, CH-8093 Zürich, Switzerland
48 University of Hamburg, D-22761 Hamburg, FRG
49 National Central University, Chung-Li, Taiwan, China
50 Department of Physics, National Tsing Hua University, Taiwan, China

§ Supported by the German Bundesministerium für Bildung, Wissenschaft, Forschung und Technologie
‡ Supported by the Hungarian OTKA fund under contract numbers T019181, F023259 and T024011.
¶ Also supported by the Hungarian OTKA fund under contract numbers T22238 and T026178.
♭ Supported also by the Comisión Interministerial de Ciencia y Tecnología.
♯ Also supported by CONICET and Universidad Nacional de La Plata, CC 67, 1900 La Plata, Argentina.
♢ Also supported by Panjab University, Chandigarh-160014, India.
△ Supported by the National Natural Science Foundation of China.

† Deceased.

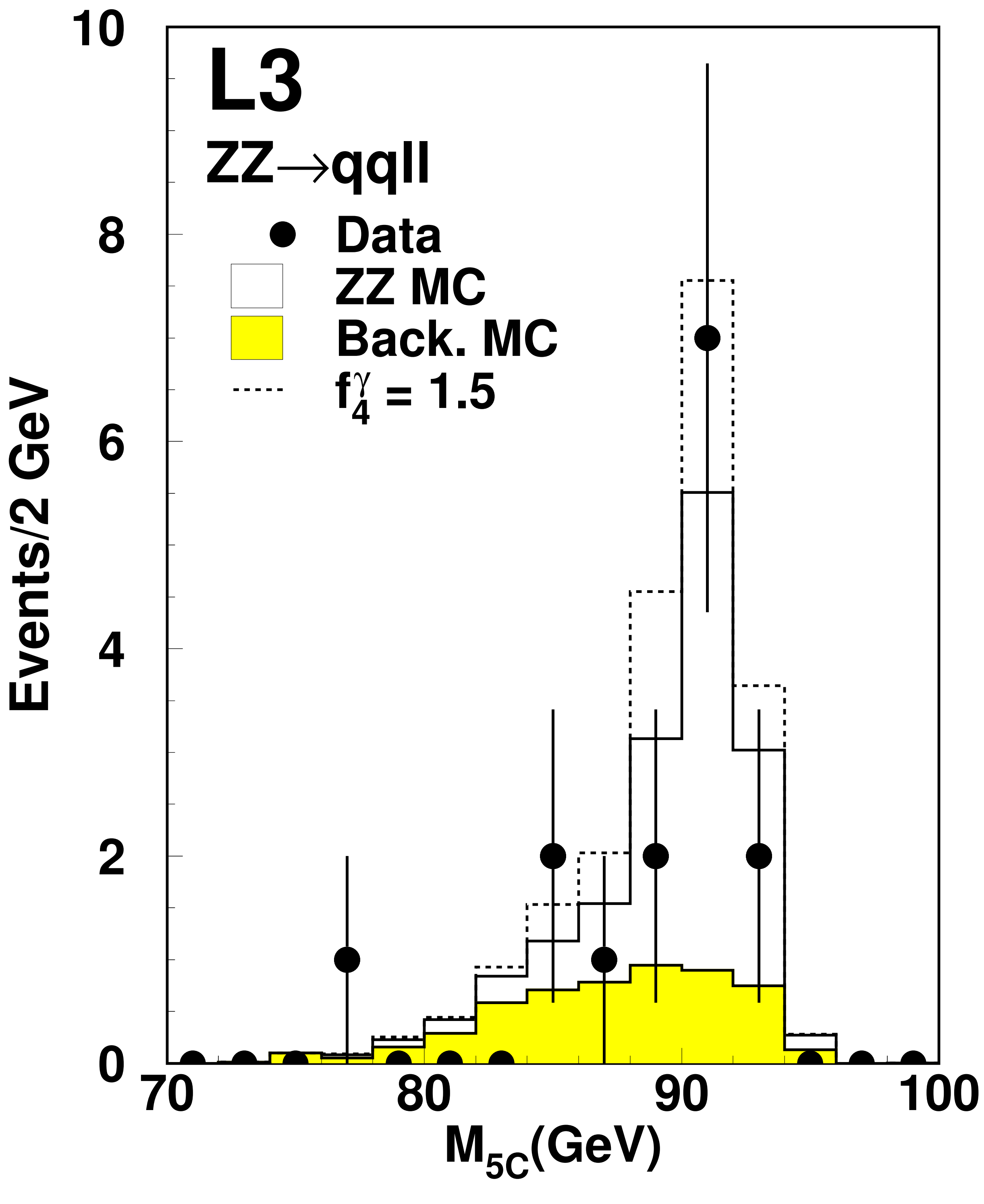

Figure 1: Invariant mass after a kinematic fit, M_{5C}, of the lepton pair for the $q\bar{q}\ell^+\ell^-$ selected events. The effect of an anomalous $ZZ\gamma$ vertex is also shown for a value of its coupling $f_4^\gamma = 1.5$.

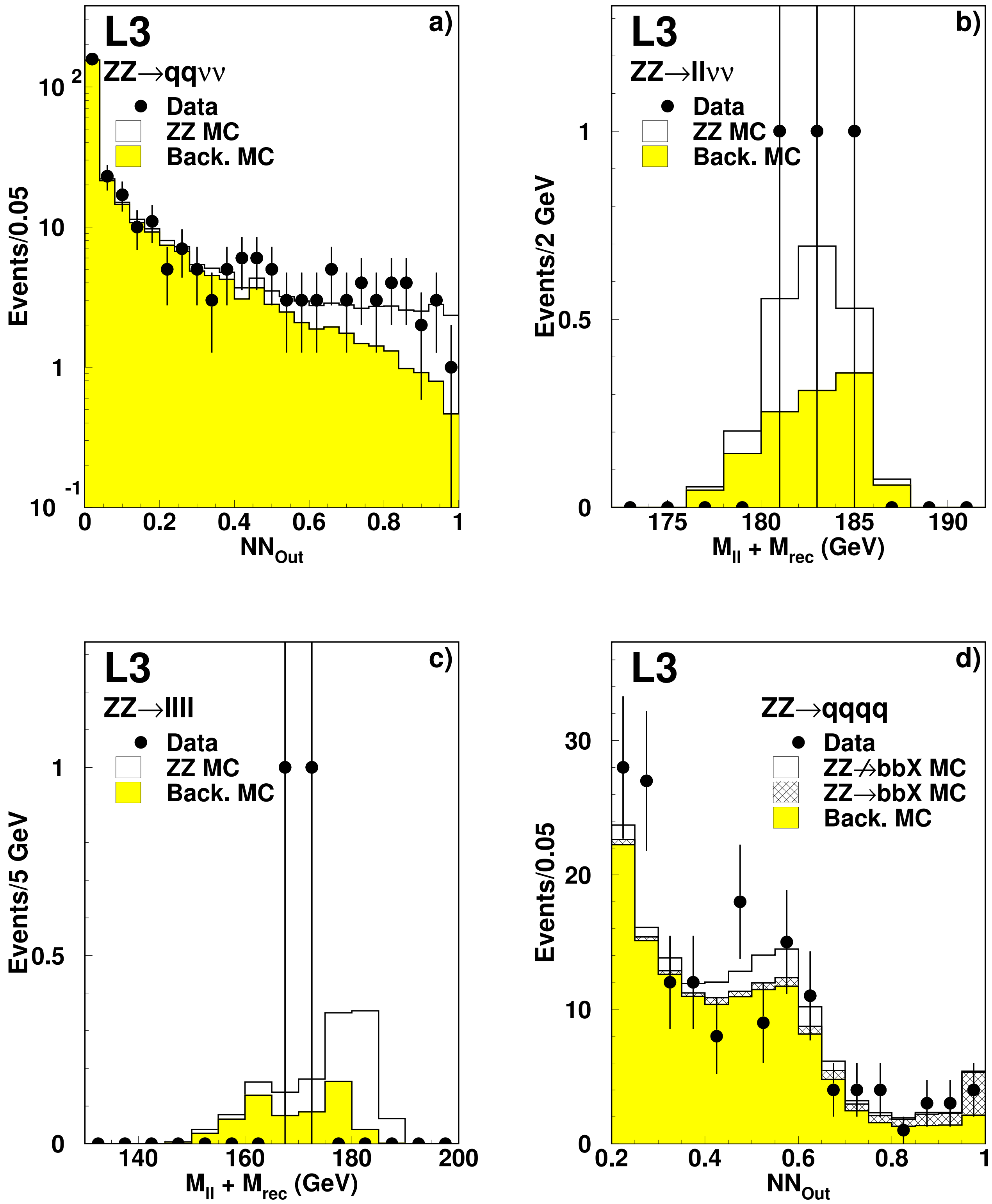

Figure 2: a) Neural network output for $\mathrm{q\bar{q}}\nu\bar{\nu}$ selected events. b) Sum of the visible and recoil masses for the events selected by the $\ell^+\ell^-\nu\bar{\nu}$ selection. c) Sum of the invariant and recoil masses of the lepton pair closest to $\mathrm{M_Z}$ for the $\ell^+\ell^-\ell'^+\ell'^-$ selected events. d) Output of the second neural network for the $\mathrm{q\bar{q}q'\bar{q}'}$ selection; signal expectations for events with no or at least one b quark pair are presented separately.

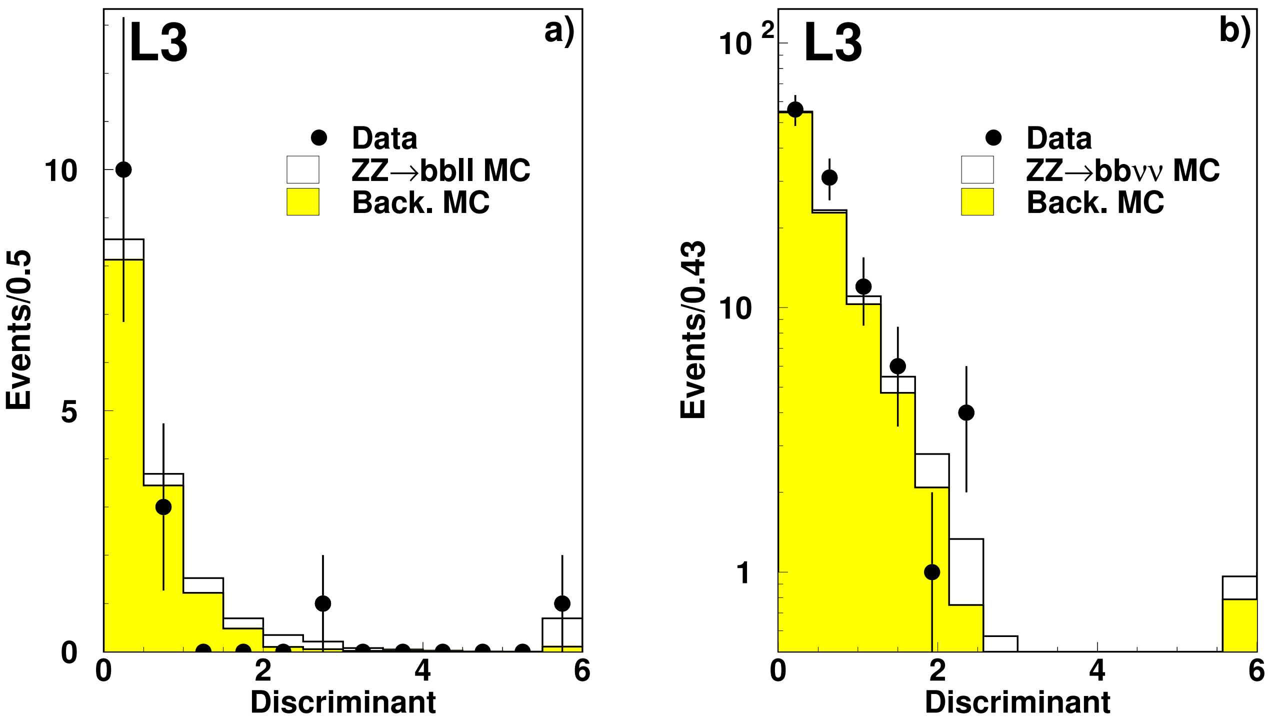

Figure 3: Discriminant variables for a) the $b\bar{b}\ell^+\ell^-$ and b) the $b\bar{b}\nu\bar{\nu}$ selections. The last bin shows the overflows.

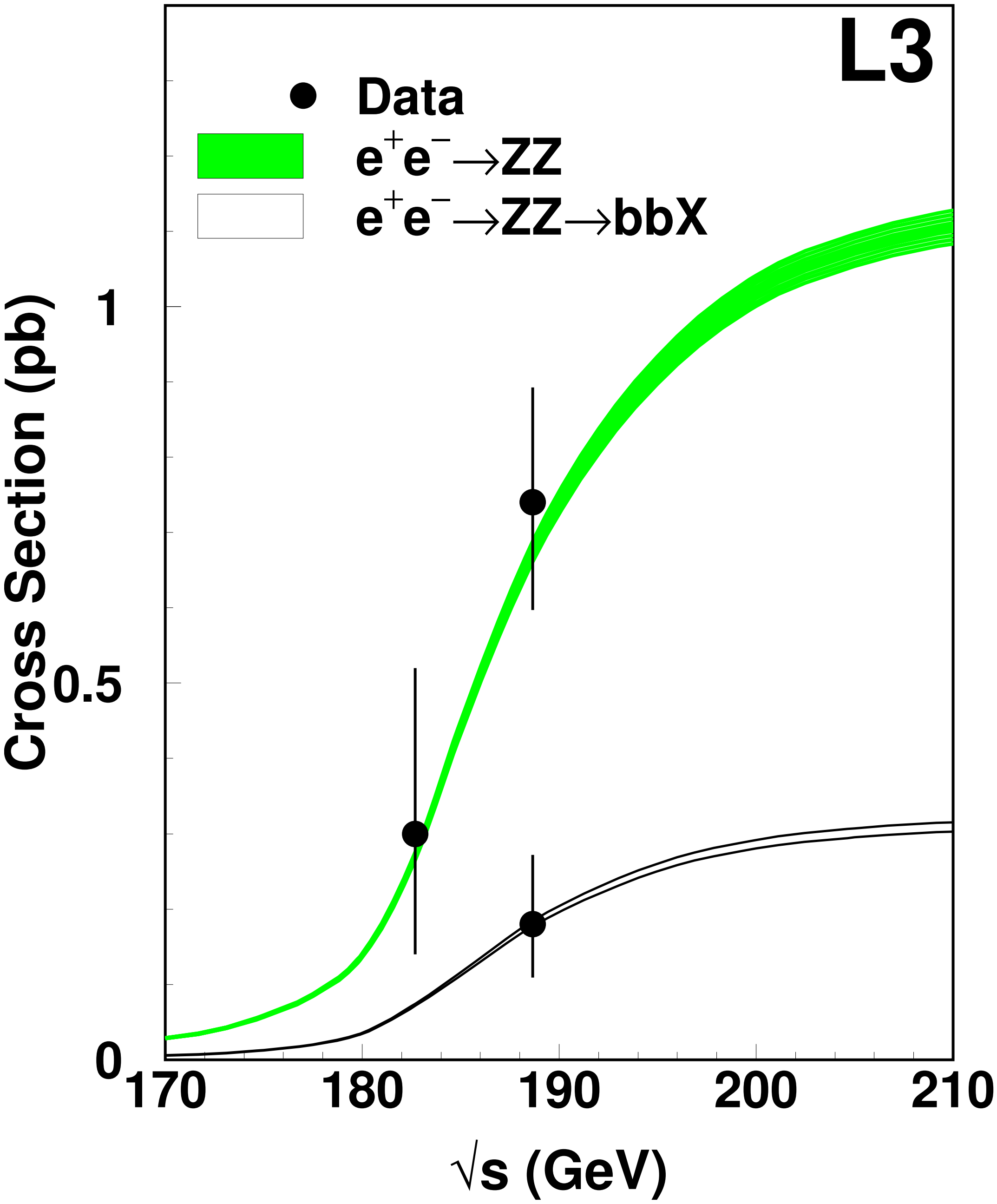

Figure 4: Standard Model prediction for the ZZ and ZZ $\rightarrow \mathrm{b\bar{b}X}$ cross sections and the corresponding measurements where statistical and systematic uncertainties are added in quadrature. Signal definition cuts implemented with the EXCALIBUR Monte Carlo are applied and a 2% uncertainty is associated to the predictions.